On areas of attraction and repulsion in finite time dynamical systems and their numerical approximation

Alina Girod* Thorsten Hüls*
Department of Mathematics, Bielefeld University,
POB 100131, 33501 Bielefeld, Germany
agirod@uni-bielefeld.de huels@math.uni-bielefeld.de

May 9, 2017

Abstract

Stable and unstable fiber bundles with respect to a fixed point or a bounded trajectory are of great dynamical relevance in (non)autonomous dynamical systems. These sets are defined via an infinite limit process. However, the dynamics of several real world models are of interest on a short time interval only. This task requires finite time concepts of attraction and repulsion that have been recently developed in the literature. The main idea consists in replacing the infinite limit process by a monotonicity criterion and in demanding the end points to lie in a small neighborhood of the reference trajectory. Finite time areas of attraction and repulsion defined in this way are fat sets and their dimension equals the dimension of the state space. We propose an algorithm for the numerical approximation of these sets and illustrate its application to several two- and three-dimensional dynamical systems in discrete and continuous time. Intersections of areas of attraction and repulsion are also calculated, resulting in finite time homoclinic orbits.

Keywords: Invariant fiber bundles, finite time dynamical systems, finite time hyperbolicity, areas of attraction and repulsion, contour algorithm, homoclinic orbits.
AMS Subject Classification: 37B55, 37D10, 34D09, 34C37.

1 Introduction

Stable and unstable fiber bundles in autonomous and nonautonomous dynamical systems on a bi-infinite time interval, consist of all points that converge in forward time respectively in backward time towards a reference solution. Due to the

*Supported by CRC 701 'Spectral Structures and Topological Methods in Mathematics'.

dynamical importance of invariant fiber bundles, various concepts have been developed for their approximation, cf. [8, 10, 14, 17, 19, 21, 23, 27, 32, 33, 38, 45, 46]. However, the infinite limit process becomes meaningless, when one is interested in short time dynamics or if the system is defined on a finite time interval only.

In this paper, we consider a nonautonomous dynamical system $(\mathbb{R}^d, \mathbb{T}, \Psi)$, where $\mathbb{T}$ denotes a finite interval of $\mathbb{R}$ or $\mathbb{Z}$. The operator $\Psi(t, s; x)$ describes the evolution of the point $x \in \mathbb{R}^d$ from time $s \in \mathbb{T}$ to time $t \in \mathbb{T}$. The evolution operator of a nonautonomous dynamical system is alternatively denoted as two-parameter semi-groups or as processes, see [37, Definition 2.1].

The reference objects for which areas of attraction are computed are hyperbolic trajectories. An appropriate concept of finite time hyperbolicity is introduced in detail in Section 2. It is based on exponential dichotomies and has been developed in [5, 6, 16].

In finite time dynamical systems, the notions *area of attraction* and *area of repulsion* allows various definitions that are not equivalent. Several authors define these sets via decay conditions, and we refer to [18] for planar nonautonomous ODEs, to [22] for nonautonomous ODEs in $\mathbb{R}^n$ and to [36] for nonautonomous processes in $\mathbb{R}^n$. Areas of attraction and repulsion are called stable and unstable manifolds in autonomous systems. Corresponding sets in the nonautonomous case are denoted as invariant stable and unstable fiber bundles, assuming they exhibit respective topological structures.

In autonomous dynamical systems, generated by two-dimensional velocity fields, Haller computed in [24] finite-time invariant manifolds via local maxima of the scalar field $d_T(x_0) = \max_{t \in [t_0, t_0+T]} \{t : \det D_x f(\Psi(\tau, t_0; x_0), \tau) < 0 \text{ for all } t_0 \leq \tau < t\}$. Contour plots of d_T provide approximations of finite time manifolds. For detecting organized structures in fluid flows, the authors of [9] compare methods that are based on manifold approximations with techniques for evaluating the finite time Lyapunov exponent field. Related techniques are based on computing contours of Lagrangian descriptors, see e.g. [40]. Alternative approaches for computing areas of attraction and repulsion are based on numerical continuation of local approximations. This ansatz is applied in [41] to nonautonomous dynamical systems, generated by aperiodic vector fields.

We introduce in this paper a related concept of finite time areas of attraction that is motivated by the definition of stable fibers in infinite time w.r.t. a bounded trajectory $\xi_{\mathbb{T}} = (\xi(t))_{t \in \mathbb{T}}$. First, we choose an $\varepsilon > 0$ and replace the condition $\lim_{t \to \infty} \Psi(t, t_0; x) - \xi(t) = 0$ by $\|\Psi(t_+, t; x) - \xi(t_+)\| \leq \varepsilon$, where $\mathbb{T} = [t_-, t_+]$. Note that a trajectory may enter and leave the ε-neighborhood of $\xi_{\mathbb{T}}$ several times. From the last entry point in $\mathbb{T}$ on, we additionally require the trajectory to decay monotonously towards $\xi_{\mathbb{T}}$ in an appropriately chosen norm. This condition reflects the fact, that in infinite time, the stable fiber of a hyperbolic trajectory consists locally of those points, whose orbits stay for all positive times in a sufficiently small neighborhood of this trajectory, see [48, Theorem III.7] for autonomous and [44, Corollary 4.6.11] for nonautonomous systems.

Areas of attraction, defined in this way, are numerically accessible and invert-

ibility assumptions on the dynamical system are not needed for their calculation. The approach that we pursue in this paper is motivated by recent contour techniques for dynamical systems in infinite time. Corresponding algorithms allow the computation of stable fibers, cf. [32, 33] as well as the detection of stable hierarchies of fiber bundles, see [34]. In contrast to the infinite time case, finite time systems do not require artificial restrictions to finite intervals in order to apply numerical algorithms. The boundaries of finite time areas of attractions turn out to be explicitly given as zero-contours of specific operators.

When dealing with areas of attraction, we do not assume invertibility of the underlying dynamical system. However, invertibility is assumed for the computation of areas of repulsion, which are areas of attraction for the inverted system. In the discrete time case, this assumption is critical, while for continuous time ODE models, invertibility is guaranteed under reasonable assumptions.

In Section 3 we introduce contour techniques for nonautonomous linear systems. The resulting algorithm is applied to several three-dimensional discrete time models. A generalization to nonlinear systems is introduced in Section 4. Furthermore, we compute areas of attraction and areas of repulsion as well as their intersections for finite time ODE models. The latter set is also accessible via contour calculations. Points in this intersection belong to finite time homoclinic orbits and we particularly discuss the dynamical relevance of homoclinic orbits in finite time dynamical systems.

2 Hyperbolic trajectories and areas of attraction and repulsion

Finite time dynamical systems

$$(\mathbb{R}^d, \mathbb{T}, \Psi) \quad \text{with} \quad \Psi \in \mathcal{C}^2(\mathbb{T} \times \mathbb{T} \times \mathbb{R}^d, \mathbb{R}^d) \tag{1}$$

are generated, for example, by nonautonomous ODEs on a continuous time interval $\mathbb{T} = [t_-, t_+]$ and by difference equations on a discrete time interval $\mathbb{T} = [t_-, t_+] \cap \mathbb{Z}$ with $t_\pm \in \mathbb{Z}$:

$$x'(t) = f(t, x(t)), \quad t \in \mathbb{T} \quad \text{respectively} \quad x(t+1) = f(t, x(t)), \quad t \in \mathbb{T}. \tag{2}$$

Ψ is the evolution operator of these systems, i.e. if $x(s) = x_0$ then $x(t) = \Psi(t, s; x_0)$ for $t, s \in \mathbb{T}$, $t \geq s$.

For $f \in \mathcal{C}^{0,1}(\mathbb{R} \times \mathbb{R}^d, \mathbb{R}^d)$ solutions of the ODE (2) locally exist in both time directions and thus, Ψ is invertible. Invertibility is generally not true, if Ψ is generated by a difference equation.

In the following, open and closed intervals in $\mathbb{T}$ are denoted by $(t, s)_\mathbb{T} = (t, s) \cap \mathbb{T}$ and $[t, s]_\mathbb{T} = [t, s] \cap \mathbb{T}$, respectively.

Let $\xi(t) = \Psi(t, t_-; \xi(t_-))$ for $t \in \mathbb{T}$ be a reference solution. We establish a notion of hyperbolicity for the trajectory $\xi_\mathbb{T} = (\xi(t))_{t \in \mathbb{T}}$ and consider for this

task the dynamical system

$$(\mathbb{R}^d, \mathbb{T}, \Phi), \quad \text{where} \quad \Phi(t,s) = D_x \Psi(t,s;\xi(s)), \quad t,s \in \mathbb{T},\ t \geq s. \tag{3}$$

If Ψ is generated by (2), then Φ is the solution operator of the corresponding variational equation

$$\begin{array}{rcll} u'(t) & = & D_x f(t,\xi(t))u(t), & t \in \mathbb{T} \quad \text{respectively} \\ u(t+1) & = & D_x f(t,\xi(t))u(t), & t \in \mathbb{T}. \end{array} \tag{4}$$

2.1 Finite time hyperbolicity

The notion of hyperbolicity considered here is based on exponential dichotomies that have been developed in [12, 13, 43]. For noninvertible systems in infinite time, we refer to [2, 28, 35]. The definition of a finite time exponential dichotomy considered here is an extension of [6, 5, 16, 36] to noninvertible systems. In the following, $\mathcal{R}(P)$ denotes the range of the projector P.

Definition 1 *The dynamical system* (3) *has an* ***exponential dichotomy*** *on* $\mathbb{T}$ *w.r.t.* $\|\cdot\|$, *if there exist constants* $\alpha_s, \alpha_u > 0$ *and families of projectors* P_t^s, $P_t^u := I - P_t^s$, $t \in \mathbb{T}$, *such that*

(i) $P_t^{s,u}\Phi(t,s) = \Phi(t,s)P_s^{s,u}$ *for all* $t,s \in \mathbb{T}$, $t \geq s$,

(ii) $\Phi(t+1,t)|_{\mathcal{R}(P_t^u)} : \mathcal{R}(P_t^u) \to \mathcal{R}(P_{t+1}^u)$ *is invertible for all* $t, t+1 \in \mathbb{T}$. *Denote the inverse of* $\Phi(t,s)|_{\mathcal{R}(P_s^u)}$ *by* $\Phi(s,t) : \mathcal{R}(P_t^u) \to \mathcal{R}(P_s^u)$, $t,s \in \mathbb{T}$, $t \geq s$.

(iii) For $t,s \in \mathbb{T}$, $t \geq s$, *the following estimates hold*

$$\begin{array}{rcll} \|\Phi(t,s)x\| & \leq & \mathrm{e}^{-\alpha_s(t-s)}\|x\| & \text{for all } x \in \mathcal{R}(P_s^s), \\ \|\Phi(s,t)x\| & \leq & \mathrm{e}^{-\alpha_u(t-s)}\|x\| & \text{for all } x \in \mathcal{R}(P_t^u). \end{array} \tag{5}$$

For dynamical systems, generated by ODE models, both systems (1) and (3) are invertible under reasonable assumptions. Thus, condition (ii) from Definition 1 is satisfied.

Unlike the infinite time case, dichotomy projectors of finite time systems are in general not unique, see [5, Example 4]. The unique objects are stable and unstable cones, cf. [16].

The choice of the norm in (5) is critical since an additional constant K on the right hand side is not permitted that may compensate for transient dynamics. Typical choices of norms are $\|x\|_\Gamma := \langle x, \Gamma x\rangle$ with a positive definite and symmetric matrix $\Gamma \in \mathbb{R}^{d,d}$. The matrix Γ may originate from a similarity transformation, since the Euclidean norm of $S\Phi(t,s)S^{-1}$ equals the Γ-norm of (3), with $\Gamma = S^TS$. For autonomous systems, $\|\cdot\|$ can alternatively be chosen to be Lyapunov adapted, cf. [3, Section 4.1]. Note that a nonautonomous choice of the norm $\|x\|_{\Gamma_t} = \langle x, \Gamma_t x\rangle$, where $\Gamma_t = S_t^TS_t$ is also possible. Selecting this

norm is particularly motivated by a nonautonomous Lyapunov transformation $S_t\Phi(t,s)S_s^{-1}$ of (3). In finite time, this concept is problematic, since transformations to arbitrary systems can be achieved in this way, see [6, Remark 7].

Due to its strict monotonicity, the dichotomy concept from Definition 1 is referred to as M-hyperbolicity in the literature. We note that further nonequivalent finite-time notions of hyperbolicity have been introduced, and connections between these spectral concepts are pointed out in [15]. We particularly mention the stronger concept of D-hyperbolicity, see [4, 25] and finite time Lyapunov exponents, see [26, 47].

2.2 Finite time areas of attraction

Let $\xi_{\mathbb{T}}$ be a trajectory of (1) that is hyperbolic, i.e. the corresponding variational equation (3) has an exponential dichotomy in the sense of Definition 1. With respect to this trajectory, we define finite time areas of attraction as follows. First, we fix $\varepsilon > 0$ and introduce a local characterization of areas of attraction in $\mathcal{B}_\varepsilon(\xi_{\mathbb{T}}) = \{x_{\mathbb{T}} : \|x_{\mathbb{T}} - \xi_{\mathbb{T}}\|_\infty \leq \varepsilon\}$. For $t \in \mathbb{T}$, $t < t_+$ we define

$$\begin{aligned}\mathcal{W}^s_{\mathrm{loc},\varepsilon}(\xi_{\mathbb{T}},t) \;:=\; &\{x \in \mathcal{B}_\varepsilon(\xi(t)) : \forall t_1,t_2 \in [t,t_+]_{\mathbb{T}},\ t_1 < t_2 : \\ &\|\Psi(t_2,t;x) - \xi(t_2)\| < \|\Psi(t_1,t;x) - \xi(t_1)\|\} \cup \{\xi(t)\}.\end{aligned} \tag{6}$$

Here, the limit condition from infinite time dynamical systems is replaced by ε-closeness and eventual monotonicity.

Orbits of the variational equation (3) converge monotonously for starting points x in the range of the stable dichotomy projector. Using the dichotomy estimate (5), it follows for all $t \in [t_-,t_+)_{\mathbb{T}}$ and all $t_1,t_2 \in [t,t_+]_{\mathbb{T}}$ with $t_1 < t_2$ that

$$\|\Phi(t_2,t)x\| = \|\Phi(t_2,t_1)\Phi(t_1,t)x\| \leq \mathrm{e}^{-\alpha_s(t_2-t_1)}\|\Phi(t_1,t)x\| < \|\Phi(t_1,t)x\|.$$

This result motivates the monotonicity condition in (6). Conversely, if we assume for fixed $t \in [t_-,t_+)_{\mathbb{T}}$ that

$$\|\Phi(t_2,t)x\| < \|\Phi(t_1,t)x\| \quad \text{for all } t_1,t_2 \in [t,t_+]_{\mathbb{T}} \text{ with } t_1 < t_2,$$

then we conclude in this linear case that $x \in \mathcal{R}(P^s_t)$, where P^s_t is a stable projector of an exponential dichotomy on $[t,t_+]_{\mathbb{T}}$.

The local area of attraction of the bounded trajectory $\xi_{\mathbb{T}}$ of the nonlinear model turns out to be tangential to the stable cone from the exponential dichotomy of the corresponding variational equation, see [36, Theorem 4.13].

Dependence on the chosen norm that we observed in Definition 1 is also critical in (6). For nonautonomous, linear models, strictly monotone convergence towards the fixed point 0 holds true globally, if all stable and unstable directions are invariant and orthogonal to each other. One can achieve this, by applying a nonautonomous Lyapunov transformation, resulting in a nonautonomous norm. However, assuming monotonicity globally is too restrictive.

We define the time, when the trajectory with starting point x at time $t \in \mathbb{T}$, defined as $\{\Psi(\ell, t; x) : \ell \in [t, t_+]_{\mathbb{T}}\}$, enters $\mathcal{B}_\varepsilon(\xi_{\mathbb{T}})$ and stays from that time on in this neighborhood:

$$m^s(\xi_{\mathbb{T}}, \varepsilon, x, t) = \inf\{s \in [t, t_+]_{\mathbb{T}} : \Psi(\ell, t; x) \in \mathcal{B}_\varepsilon(\xi(\ell)) \forall \ell \in [s, t_+]_{\mathbb{T}}\}, \tag{7}$$

where $\inf \emptyset := t_+$.

Our global version of the finite time area of attraction reads for $t \in \mathbb{T}$, $t < t_+$

$$\begin{aligned} \mathcal{W}^s_\varepsilon(\xi_{\mathbb{T}}, t) \;:=\; & \{x \in \mathbb{R}^d : s = m^s(\xi_{\mathbb{T}}, \varepsilon, x, t) \in [t, t_+)_{\mathbb{T}} \\ & \text{and } \Psi(s, t; x) \in \mathcal{W}^s_{\mathrm{loc},\varepsilon}(\xi_{\mathbb{T}}, s)\}. \end{aligned} \tag{8}$$

The definition of (8) mimics the construction of the global stable manifold via a continuation process, starting with a local graph representation. Observe that the evolution operator Ψ does not have to be invertible in order to define (8). In (8), the length of the finite time area of attraction depends on ε. The following lemma describes its dependence on ε.

Lemma 2 *Assume that $\xi_{\mathbb{T}}$ is a hyperbolic trajectory of (1) and fix $t \in [t_-, t_+)_{\mathbb{T}}$.*

(i) Let $\varepsilon_1 > \varepsilon_2 > 0$, then $\mathcal{W}^s_{\mathrm{loc},\varepsilon_1}(\xi_{\mathbb{T}}, t) \supset \mathcal{W}^s_{\mathrm{loc},\varepsilon_2}(\xi_{\mathbb{T}}, t)$.

(ii) Let $\varepsilon_1 > \varepsilon_2 > 0$, $x \in \mathcal{W}^s_{\varepsilon_1}(\xi_{\mathbb{T}}, t)$ and assume that $m^s(\xi_{\mathbb{T}}, \varepsilon_2, x, t) \in [t, t_+)_{\mathbb{T}}$, then $x \in \mathcal{W}^s_{\varepsilon_2}(\xi_{\mathbb{T}}, t)$.

Areas of attraction are positive invariant in the following sense:

Lemma 3 *Assume that $\xi_{\mathbb{T}}$ is a hyperbolic trajectory of (1) and fix $\varepsilon > 0$, $t \in [t_-, t_+)_{\mathbb{T}}$.*

(i) Let $x \in \mathcal{W}^s_{\mathrm{loc},\varepsilon}(\xi_{\mathbb{T}}, t)$, then $\Psi(s, t; x) \in \mathcal{W}^s_{\mathrm{loc},\varepsilon}(\xi_{\mathbb{T}}, s)$ for all $s \in [t, t_+)_{\mathbb{T}}$.

(ii) Let $x \in \mathcal{W}^s_\varepsilon(\xi_{\mathbb{T}}, t)$, then $\Psi(s, t; x) \in \mathcal{W}^s_\varepsilon(\xi_{\mathbb{T}}, s)$ for all $s \in [t, t_+)_{\mathbb{T}}$.

2.3 Finite time areas of repulsion

Assuming that the dynamical system (1) is invertible, we observe that areas of repulsion are areas of attraction of the inverse system. Thus, one can define $W^u_{\mathrm{loc},\varepsilon}$, W^u_ε and m^u in complete analogy to (6), (8) and (7). The version that we introduce here is more general and applies to noninvertible systems, too, since the evolution operator Ψ is evaluated forward in time only. Let

$$\begin{aligned} \mathcal{W}^u_\varepsilon(\xi_{\mathbb{T}}, t) \;:=\; & \{x \in \mathbb{R}^d : \exists y \in \mathbb{R}^d : \Psi(t, t_-; y) = x \text{ and} \\ & s = m^u(\xi_{\mathbb{T}}, \varepsilon, y, t) \in (t_-, t]_{\mathbb{T}} \text{ and } \forall t_1, t_2 \in [t_-, s]_{\mathbb{T}}, t_2 < t_1 : \\ & \|\Psi(t_2, t_-; y) - \xi(t_2)\| < \|\Psi(t_1, t_-; y) - \xi(t_1)\|\} \cup \{\xi(t)\}, \end{aligned}$$

with

$$m^u(\xi_{\mathbb{T}}, \varepsilon, y, t) = \sup\{s \in [t_-, t]_{\mathbb{T}} : \Psi(\ell, t_-; y) \in \mathcal{B}_\varepsilon(\xi(\ell)) \forall \ell \in [t_-, s]_{\mathbb{T}}\},$$

where $\sup \emptyset := t_-$.

3 Linear systems, areas of attraction and their computation

In this section, we consider linear dynamical systems $(\mathbb{R}^d, \mathbb{T}, \Phi)$ that are finite time hyperbolic in the sense of Definition 1. An important example within this class of systems is the variational equation (3), (4) w.r.t. a hyperbolic trajectory.

On a bi-infinite time interval $\mathbb{T}$, one compensates for transient dynamics by allowing a constant $K \geq 1$ on the right hand sides of the dichotomy estimates (5). Furthermore, dichotomy projectors are uniquely determined in infinite time, see [42]. Stable and unstable fiber bundles turn out to be the ranges of corresponding stable respectively unstable dichotomy projectors. Techniques for the numerical approximation of dichotomy projectors have been proposed in [29, 30]. The corresponding algorithms are based on solving least squares and boundary value problems.

To finite time systems, these techniques are not directly applicable, due to the non-uniqueness of dichotomy projectors. The unique objects, one is interested in, are stable and unstable cones, cf. [16]. We define the stable cone for $t \in [t_-, t_+)_{\mathbb{T}}$ as follows

$$\mathcal{M}^s(t) := \{x \in \mathbb{R}^d : \forall t_1, t_2 \in [t, t_+]_{\mathbb{T}}, t_1 < t_2 : \|\Phi(t_2, t)x\| < \|\Phi(t_1, t)x\|\} \cup \{0\} \tag{9}$$

and observe the following connection between stable cones and areas of attraction:

$$\mathcal{M}^s(t) \cap \mathcal{B}_\varepsilon(0) = \mathcal{W}^s_{\mathrm{loc},\varepsilon}(0_{\mathbb{T}}, t) \quad \text{for all } \varepsilon > 0.$$

Note that $\mathcal{M}^s(t)$ does generally not define the stable cone of the finite time dichotomy in the sense of [16, Section 3], which requires monotonicity on $[t_-, t_+]_{\mathbb{T}}$ rather than on $[t, t_+]_{\mathbb{T}}$ as in (9).

3.1 Numerical approximation in the linear case

In order to derive a numerical algorithm, we assume that $\mathbb{T}$ is a discrete set. Note that hyperbolic continuous time dynamical systems turn into hyperbolic discrete time systems when considered on a discrete subset $\{t_{n_-}, \ldots, t_{n_+}\}$ of $\mathbb{T}$. But for concrete ODE-models, the corresponding t-flow is typically not known explicitly. Then, a one-step discretization scheme provides the required discrete time data.

On $\mathbb{T} = \{t_{n_-}, \ldots, t_{n_+}\}$, (9) reads for $n \in [n_-, n_+ - 1]_{\mathbb{Z}}$

$$\mathcal{M}^s(t_n) = \{x \in \mathbb{R}^d : \forall \ell \in [n, n_+ - 1]_{\mathbb{Z}} : \|\Phi(t_{\ell+1}, t_n)x\| < \|\Phi(t_\ell, t_n)x\|\}. \tag{10}$$

We observe that $\partial\mathcal{M}^s(t_n) \subset \mathcal{J}^s(t_n)$ for $n \in [n_-, n_+ - 1]_{\mathbb{Z}}$, where

$$\begin{aligned} \mathcal{J}^s(t_n) &= \{x \in \mathbb{R}^d : g_n(x) = 0\}, \\ g_n(x) &= \max_{\ell \in [n, n_+ - 1]_{\mathbb{Z}}} (\|\Phi(t_{\ell+1}, t_n)x\| - \|\Phi(t_\ell, t_n)x\|). \end{aligned}$$

For $d = 2$ dimensional systems, we numerically calculate $\mathcal{J}^s(t_n)$, i.e. the zero contour of g_n, for x in some rectangle, using the MATLAB-command `contour`.

For a $d = 3$ dimensional model we similarly compute an approximation of $\mathcal{J}^s(t_n)$ on some cuboid using the MATLAB-command `isosurface`. The input of these MATLAB-functions is a value table of g_n w.r.t. a discretization of the rectangle respectively cuboid. In higher dimensional systems, this approach allows the computation of two- and three-dimensional projections of $\mathcal{J}^s(t_n)$.

3.2 Autonomous linear models

We consider the autonomous linear case $\Phi(t,s) = A^{t-s}$ for $t, s \in \mathbb{T} = [n_-, n_+]_{\mathbb{Z}}$, $t \geq s$ with some hyperbolic matrix $A \in \mathbb{R}^{d,d}$. Assuming that A is diagonalizable, one only has to verify the condition (10) for the last step

$$\|\Phi(t_{n_+}, t)x\|_\Gamma < \|\Phi(t_{n_+-1}, t)x\|_\Gamma$$

in order to prove that $x \in \mathcal{M}^s(t)$ w.r.t. a Lyapunov adapted Γ-norm. Here

$$\Gamma = S^T S, \quad \text{where} \quad SAS^{-1} = \operatorname{diag}(\lambda_1, \ldots, \lambda_d) \tag{11}$$

with eigenvalues $\lambda_1, \ldots, \lambda_d$ of A. As described at the end of Section 2.1 the corresponding norm is given as $\|x\|_\Gamma^2 := \langle x, \Gamma x\rangle$. The following lemma justifies this simplification.

Lemma 4 *Let $A \in \mathbb{R}^{d,d}$ be diagonalizable and hyperbolic. Let $N \in \mathbb{N}$, $x \in \mathbb{R}^d$ and assume that $\|A^{N+1}x\|_\Gamma < \|A^N x\|_\Gamma$. Then $\|A^{\ell+1}x\|_\Gamma < \|A^\ell x\|_\Gamma$ for all $\ell = 0, \ldots, N$.*

Proof: Fix $x \in \mathbb{R}^d$ and note that $\|Ax\|_\Gamma^2 = \|SAS^{-1}Sx\|_2^2 = \sum_{i=1}^d \lambda_i^2 (Sx)_i^2$, where $(Sx)_i$ denotes the i-th component of Sx.

We prove the converse statement $\|x\|_\Gamma \leq \|Ax\|_\Gamma \Rightarrow \|Ax\|_\Gamma \leq \|A^2x\|_\Gamma$ which yields the claim inductively.

Assuming $\|x\|_\Gamma \leq \|Ax\|_\Gamma$ it follows that

$$\begin{aligned} 0 \geq \|x\|_\Gamma^2 - \|Ax\|_\Gamma^2 &= \sum_{i=1}^d (1-\lambda_i^2)(Sx)_i^2 \\ &= \sum_{i=1}^d \lambda_i^2(1-\lambda_i^2)(Sx)_i^2 + \sum_{i=1}^d (1-\lambda_i^2)^2 (Sx)_i^2. \end{aligned}$$

As a consequence

$$0 \geq \sum_{i=1}^d \lambda_i^2(1-\lambda_i^2)(Sx)_i^2 = \|Ax\|_\Gamma^2 - \|A^2x\|_\Gamma^2.$$

■

For an illustration, we consider the three examples

$$A_1 = \begin{pmatrix} 0.9 & 0 & 0 \\ 0 & 1.1 & 0 \\ 0 & 0 & 1.5 \end{pmatrix}, \quad A_2 = \begin{pmatrix} 0.9 & 0 & 0 \\ 0 & 0.8 & 0 \\ 0 & 0 & 1.5 \end{pmatrix}, \quad A_3 = \begin{pmatrix} 0.9 & 0 & 0 \\ 0 & 0 & 0 \\ 0 & 0 & 1.5 \end{pmatrix}. \tag{12}$$

For these examples, we compute the stable cones $\mathcal{M}^s(t)$ for $t \in \{n_+ - 3, n_+ - 2, n_+ - 1\}$ in Figure 1. Note that these models are autonomous and $\mathcal{M}^s(t)$ only depends on the distance from t to the right boundary n_+ of the finite interval. The actual choices of n_+ and t are therefore irrelevant.

The noninvertibility in the third case causes for $t \in \mathbb{T}$, $t \leq n_+ - 2$ degenerate stable cones $\mathcal{M}^s(t)$. Components in x_2-direction are zero after one iteration step. If, in addition $x_1 = 0$, then the monotonicity condition in (9) is violated in the next iteration steps if $x_3 \neq 0$.

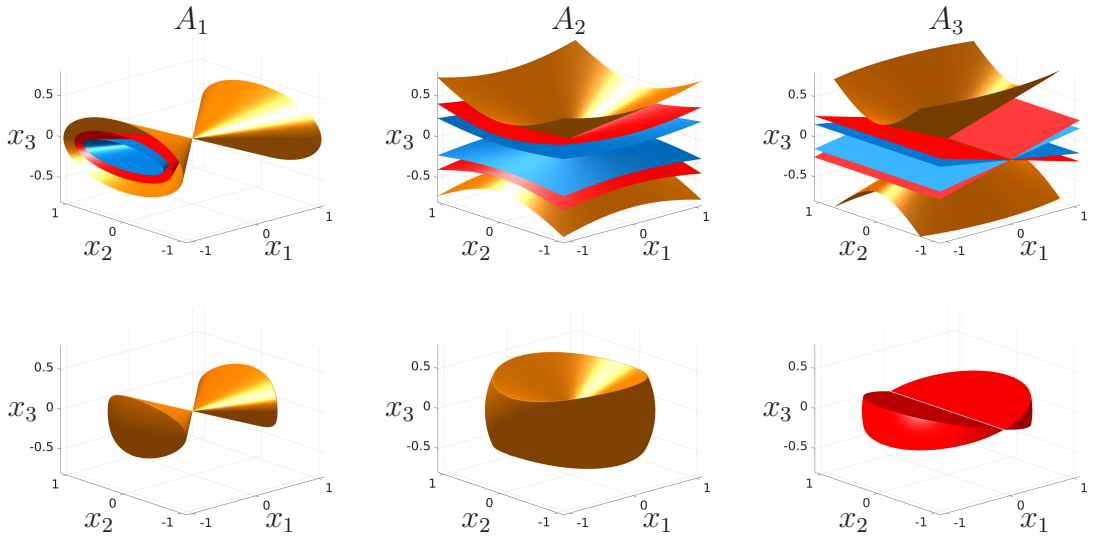

Figure 1: Upper row: Boundaries of stable cones $\mathcal{M}^s(n_+-1)$ (brown), $\mathcal{M}^s(n_+-2)$ (red), $\mathcal{M}^s(n_+ - 3)$ (blue) for the three examples (12). Lower row: Intersection of the unit sphere with $\mathcal{M}^s(n_+ - 1)$ for $A_{1,2}$ and with $\mathcal{M}^s(n_+ - 2)$ for A_3.

3.3 Nonautonomous linear models

We observed for autonomous models in Lemma 4 that it suffices to analyze monotonicity in the last step of an iteration to ensure monotonicity in each step. However, Lemma 4 does not apply to nonautonomous models. The nonautonomous case requires to verify monotonicity in each step. For an illustration, we consider the following system in discrete time

$$u(n+1) = A(n)u(n), \quad \text{where } A(n) = D(n+1) \cdot B \cdot D(-n), \tag{13}$$

$$B = \begin{pmatrix} 0.9 & 0 & 0 \\ 0 & 0.95 & 0 \\ 0 & 0 & 1.1 \end{pmatrix}, \quad D(n) = \begin{pmatrix} \cos n\varphi & 0 & -\sin n\varphi \\ \sin n\varphi & 0 & \cos n\varphi \\ 0 & 1 & 0 \end{pmatrix}, \quad \varphi = \frac{\pi}{3}.$$

We note that system (13) is not a nonautonomous similarity transformation of the constant system $v(n+1) = Bv(n)$, since $D(-n)D(n) \neq I$. Thus, the eigenvalues of $A(n)$, $n \in \mathbb{T}$ are meaningless for an analysis of the stability behavior of the fixed point 0. We refer to [20, Example 4.17] and [11, Section 2.6] for counterexamples in discrete and continuous time. Indeed, the stable subspace of the exponential dichotomy on $\mathbb{Z}$ of (13) turns out be one-dimensional.

With respect to the finite interval $\mathbb{T} = [1, 11]_{\mathbb{Z}}$ we compute the stable cones $\mathcal{M}^s(t)$ for $t \in \{3, 4, 5, 7, 9, 10\}$ in Figure 2. This figure particularly illustrates that each half of the stable (and unstable) cone is generally not convex.

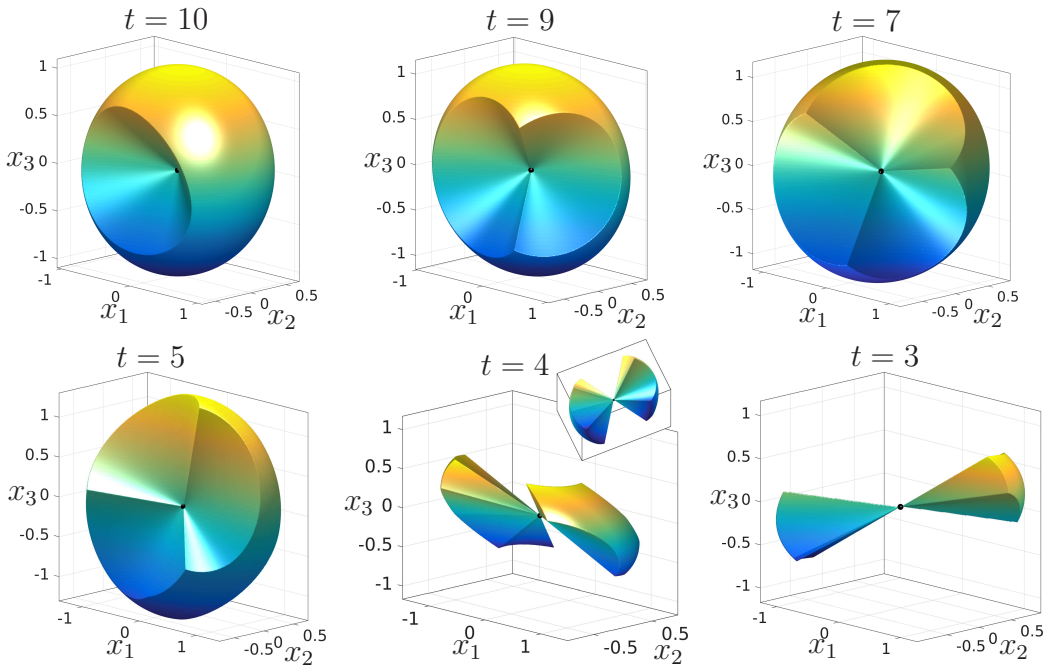

Figure 2: Intersection of the Euclidean unit-ball with stable cones $\mathcal{M}^s(t)$ of (13). For $t = 4$, an alternative view of the cone is presented.

4 Nonlinear systems, areas of attraction and repulsion and their computation

In this section, the contour techniques from Section 3 are transferred to nonlinear dynamical systems, starting with the autonomous case.

4.1 Autonomous nonlinear models

Consider the autonomous nonlinear case $\Psi(t,s;\cdot) = f^{t-s}(\cdot)$ for $t,s \in \mathbb{T} = \{t_{n_-},\dots,t_{n_+}\}$, $t \geq s$. We define $t_n = n$, if the underlying system is discrete and generated by the map f. If the underlying system is an ODE, $\mathbb{T}$ defines some grid in $\mathbb{R}$ and f is the corresponding one-step map that originates from a numerical discretization scheme.

We assume that

(A0) $f \in \mathcal{C}^2(\mathbb{R}^d,\mathbb{R}^d)$, $f(0)=0$ and $A := Df(0)$ is a hyperbolic matrix.

As in Section 3.2, we additionally assume that A is diagonalizable in order to define Γ as in (11). Also in this nonlinear setup, we obtain for sufficiently small ε that $x \in \mathcal{W}^s_{\mathrm{loc},\varepsilon}(t)$ for $x \in \mathcal{B}_\varepsilon(0)$, provided $\|\Psi(t_{n_+},t;x)\|_\Gamma < \|\Psi(t_{n_+-1},t;x)\|_\Gamma$ holds true. Thus we do not have to verify monotonicity in each step of the iteration within (6).

Lemma 5 *Assume (A0), let A be diagonalizable and fix $N \in \mathbb{N}$. Then there exists an $\varepsilon > 0$ such that for each $x \in \mathcal{B}_\varepsilon(0)$, satisfying $\|f^{N+1}(x)\|_\Gamma < \|f^N(x)\|_\Gamma$ it follows for any $\ell \in \{0,\dots,N\}$ with $f^i(x) \in \mathcal{B}_\varepsilon(0)$, $i=\ell,\dots,N$ that*

$$\|f^{\ell+1}(x)\|_\Gamma < \|f^\ell(x)\|_\Gamma.$$

Proof: First, observe that $\|f(x)\|_\Gamma^2 = \|Ax\|_\Gamma^2 + g_1(x)$ and $\|f^2(x)\|_\Gamma^2 = \|A^2x\|_\Gamma^2 + g_2(x)$ with $g_{1,2}(x) = \mathcal{O}(\|x\|_\Gamma^3)$.

Choose $\varepsilon > 0$ such that

$$\sum_{i=1}^d (1-\lambda_i^2)^2 (Sx)_i^2 \geq 2g_1(x) - g_2(x) \quad \text{for all } x \in \mathcal{B}_\varepsilon(0). \tag{14}$$

Similar to the proof of Lemma 4, we show the converse statement.

Let $x \in \mathcal{B}_\varepsilon(0)$ such that $\|x\|_\Gamma - \|f(x)\|_\Gamma \leq 0$ then $\|f(x)\|_\Gamma - \|f^2(x)\|_\Gamma \leq 0$,

which yields the claim inductively.

Assuming $\|x\|_\Gamma \leq \|f(x)\|_\Gamma$ it follows that

$$\begin{aligned} 0 \geq \|x\|_\Gamma^2 - \|f(x)\|_\Gamma^2 &= \|x\|_\Gamma^2 - \|Ax\|_\Gamma^2 - g_1(x) \\ &= \sum_{i=1}^d \lambda_i^2(1-\lambda_i^2)(Sx)_i^2 + \sum_{i=1}^d (1-\lambda_i^2)^2(Sx)_i^2 - g_1(x). \end{aligned}$$

Using (14), we conclude for $x \in \mathcal{B}_\varepsilon(0)$ that

$$0 \geq \sum_{i=1}^d \lambda_i^2(1-\lambda_i^2)(Sx)_i^2 + g_1(x) - g_2(x) = \|f(x)\|_\Gamma^2 - \|f^2(x)\|_\Gamma^2.$$

■

In the autonomous case, Lemma 5 allows in an appropriate norm $\|\cdot\|$ and for sufficiently small $\varepsilon > 0$ the efficient approximation of $\mathcal{W}^s_\varepsilon(0,t)$. First we define for $t \in [t_{n_-}, t_{n_+-1}]_{\mathbb{T}}$

$$\tilde{G}^s(z,t) := \|\Psi(t_{n_+-1}, t; z)\| - \|\Psi(t_{n_+}, t; z)\|. \tag{15}$$

By including the condition $\|\Psi(t_{n_+-1}, t; z)\| < \varepsilon$ into the operator, we obtain

$$G^s_\varepsilon(z,t) := \min\{\tilde{G}^s(z,t), \varepsilon - \|\Psi(t_{n_+-1}, t; z)\|\}. \tag{16}$$

The boundary of $\mathcal{W}^s_\varepsilon(0,t)$ is a subset of the zero-contour of $G^s_\varepsilon(\cdot,t)$ and equality holds true, if the system satisfies certain nondegeneracy conditions.

If the system is invertible, we similarly obtain an approximation of the area of repulsion for $t \in [t_{n_-+1}, t_{n_+}]_{\mathbb{T}}$ by computing the zero-contour of

$$G^u_\varepsilon(z,t) := \min\{\|\Psi(t_{n_-+1}, t; z)\| - \|\Psi(t_{n_-}, t; z)\|, \varepsilon - \|\Psi(t_{n_-+1}, t; z)\|\}. \tag{17}$$

Note that areas of repulsion are introduced in Section 2.3 for both, invertible and noninvertible systems. We avoid the time consuming search for appropriate pre-images and numerically compute in this paper areas of repulsion for invertible examples only.

Finally, we consider homoclinic areas, which are the intersections of areas of attraction and repulsion, see Section 4.1.5 for a formal introduction. This set turns out to be numerically accessible at time $t \in [t_{n_-+1}, t_{n_+-1}]_{\mathbb{T}}$ by computing the zero-contour of

$$G_\varepsilon(z,t) := \min\{G^s_\varepsilon(z,t), G^u_\varepsilon(z,t)\}. \tag{18}$$

4.1.1 A three-dimensional map with one stable eigenvalue

For an illustration, we consider the system $x(n+1) = f(x(n))$, where

$$f\begin{pmatrix} x_1 \\ x_2 \\ x_3 \end{pmatrix} = \begin{pmatrix} \frac{1}{2}x_1 \\ 2x_2 - \frac{7}{4}x_1^2 \\ 3x_3 - \frac{11}{4}x_1^2 \end{pmatrix}. \tag{19}$$

On an infinite time interval, the one-dimensional stable manifold of the hyperbolic fixed point 0 has the global graph representation

$$\mathcal{W}^s(0) = \left\{(y, y^2, y^2)^T : y \in \mathbb{R}\right\}. \tag{20}$$

We compute the boundary of $\mathcal{W}^s_\varepsilon(0,t)$ for $\varepsilon = 0.2$ and $t \in \{n_+-3, n_+-2, n_+-1\}$ in Figure 3. For this task, we evaluate for all starting points on a $400\times400\times400$ grid around the fixed point, the function $\tilde{G}^s_\varepsilon(\cdot,t)$, defined in (15). From the resulting data, the MATLAB routine `isosurface` computes the zero-contour, shown in Figure 3. We observe that for decreasing t, the approximation of $\mathcal{W}^s_\varepsilon(0,t)$ becomes longer and narrower. These three-dimensional sets converge towards the one-dimensional manifold (20) as $t \to -\infty$.

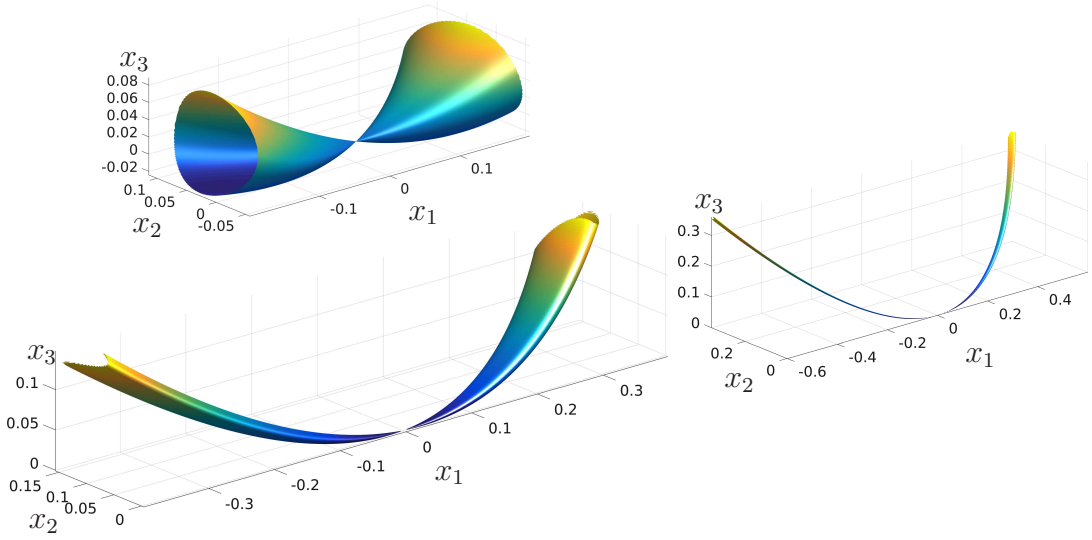

Figure 3: Approximation of $\mathcal{W}^s_\varepsilon(0,t)$ for (19) for $t = n_+ - 1$ (upper diagram), $t = n_+ - 2$ (lower diagram) and $t = n_+ - 3$ (right diagram).

4.1.2 A three-dimensional map with two stable eigenvalues

Next, we analyze the dynamical system $x(n+1) = f(x(n))$ that is generated by

$$f\begin{pmatrix} x_1 \\ x_2 \\ x_3 \end{pmatrix} = \begin{pmatrix} \frac{1}{2}x_1 \\ \frac{1}{3}x_2 \\ 2x_3 - \frac{7}{4}x_1^2 - \frac{17}{9}x_2^2 \end{pmatrix}. \tag{21}$$

The hyperbolic fixed point 0 possesses two stable and one unstable eigenvalue. When considering this system on an infinite time frame, the stable manifold has the global graph representation

$$\mathcal{W}^s(0) = \{(y_1, y_2, y_1^2 + y_2^2)^T, y \in \mathbb{R}^2\}. \tag{22}$$

We detect the boundary of $\mathcal{W}^s_\varepsilon(0,t)$ for $\varepsilon = 0.2$ and $t \in \{n_+ - 3, n_+ - 2, n_+ - 1\}$. For all points z from a $400 \times 400 \times 400$ grid we evaluate $G^s_\varepsilon(z,t)$, see (16). Zero-contours of $G^s_\varepsilon(\cdot,t)$, computed with the MATLAB routine `isosurface`, are shown in Figure 4. We observe that these three-dimensional finite time areas of attraction converge towards the two-dimensional manifold (22) as $t \to -\infty$.

4.1.3 Areas of attraction and repulsion for a two-dimensional ODE-model

We consider the finite time ODE-model

$$\begin{pmatrix} x_1 \\ x_2 \end{pmatrix}' = \begin{pmatrix} 1.6(x_1 + x_2^2) \\ \nu(-x_1^2 + x_2) \end{pmatrix}, \quad \nu = -1.6016, \quad \text{for } t \in \mathbb{T} = [-2.5, 2.5]. \tag{23}$$

This model exhibits homoclinic dynamics in finite time, since – as we will see – areas of attraction and repulsion of the hyperbolic fixed point 0 intersect. We

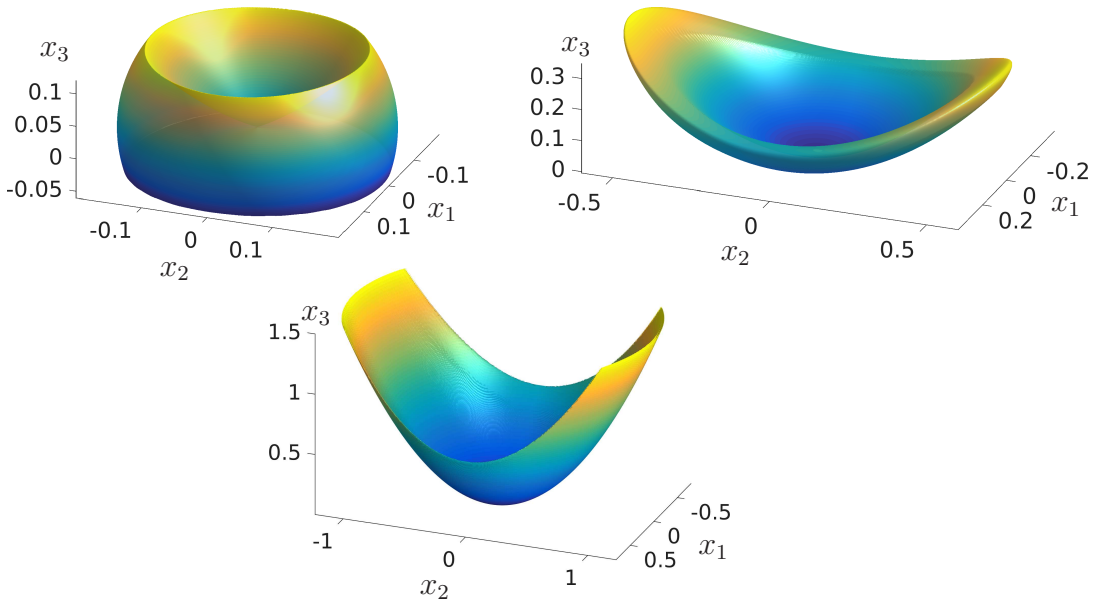

Figure 4: Approximation of $\mathcal{W}^s_\varepsilon(0,t)$ for (21) for $t = n_+ - 1$ (upper left diagram), $t = n_+ - 2$ (upper right diagram) and $t = n_+ - 3$ (lower diagram).

note that on an infinite time axis, (23) exhibits homoclinic orbits only for the parameter value $\nu = -1.6$, since for this choice of parameter, stable and unstable manifolds of the fixed point 0 have a whole orbit in common.

We discretize (23) with the classical Runge-Kutta scheme – which is a one-step method of order 4 – with step size $h = 0.01$. The area of repulsion coincides with the area of attraction for the inverse system. In the continuous time system (23), this inversion is not critical and in practice, we apply the numerical scheme with a negative step size.

We proceed by computing the zero-contour of $G^{s,u}_\varepsilon(\cdot,t)$ with $\varepsilon = 0.1$, cf. (16), (17), on a 1000×1000 grid, using the MATLAB routine `contour`. Finite time homoclinic points lie in the intersection of areas of attraction and repulsion, shown in yellow in Figure 5. The boundary of this set is given as the zero-contour of the operator $G_\varepsilon(\cdot,t)$, defined in (18). Additionally, we apply in a neighborhood of the fixed point the contour-algorithm from [32, 33] for computing nearly one-dimensional parts of areas of attraction and repulsion. We refer to the end of Section 4.2 for more details on numerical difficulties that we observe in this case.

4.1.4 A three-dimensional ODE-model with finite time homoclinic orbits

We illustrate that the techniques from Section 4.1.3 are not restricted to two-dimensional models. Consider the three-dimensional version of (23)

$$\begin{pmatrix} x_1 \\ x_2 \\ x_3 \end{pmatrix}' = \begin{pmatrix} 1.6(x_1 + x_2^2) \\ \nu(-x_1^2 + x_2) \\ 0.01 x_3 \end{pmatrix}, \quad \nu = -1.6016, \quad \text{for } t \in \mathbb{T} = [-2.5, 2.5]. \tag{24}$$

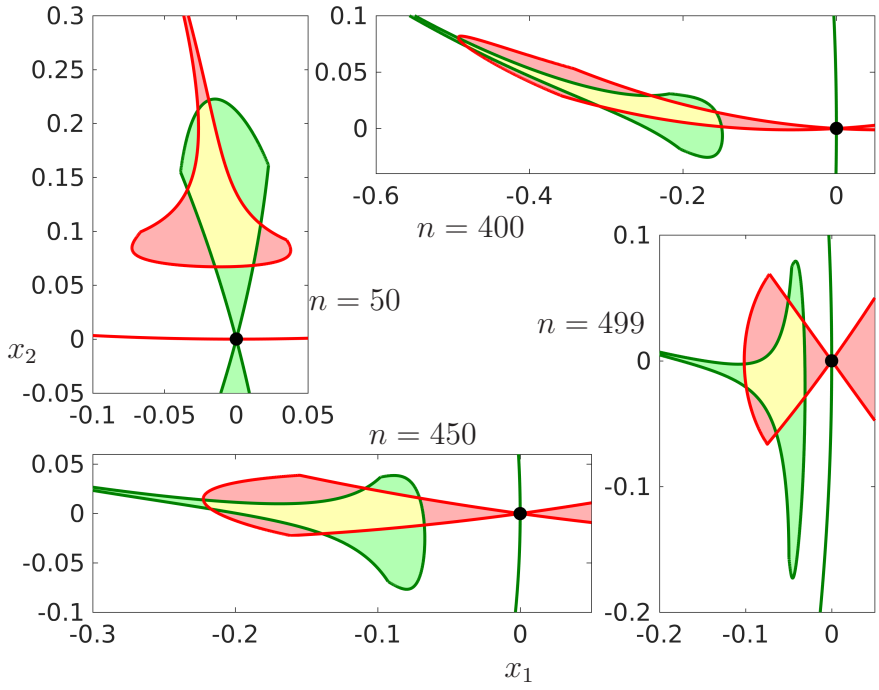

Figure 5: Approximation of $\mathcal{W}^s_\varepsilon(0,t)$ (green) and of $\mathcal{W}^u_\varepsilon(0,t)$ (red) with $t = -2.5+nh$ for (23). Homoclinic points lie in the intersection of these sets (yellow).

Using the same approach as in Section 4.1.3 we compute in Figure 6 the three-dimensional analog of the lower right diagram from Figure 5. For this task, we choose $\varepsilon = 0.1$, $h = 0.01$, $t = 2.5 - h$ and apply the `isosurface` algorithm, w.r.t. a $400 \times 400 \times 400$ grid, to $G^s_\varepsilon(\cdot,t)$, $G^u_\varepsilon(\cdot,t)$ respectively $G_\varepsilon(\cdot,t)$.

4.1.5 A note on homoclinic dynamics

Let $\xi_{\mathbb{T}}$ be a bounded trajectory of the dynamical system $(\mathbb{R}^d, \mathbb{T}, \Psi)$ on a bi-infinite time interval $\mathbb{T}$. A second trajectory $\bar{x}_{\mathbb{T}} \neq \xi_{\mathbb{T}}$ is homoclinic w.r.t. $\xi_{\mathbb{T}}$ if $\lim_{t\to\pm\infty, t\in\mathbb{T}} \|\bar{x}(t) - \xi(t)\| = 0$. Under reasonable hyperbolicity assumptions, numerical approximations of $\xi_{\mathbb{T}}$ and $\bar{x}_{\mathbb{T}}$ can be computed by solving boundary value problems. Precise error estimates justify the approximation process, see [7, Section 4] for autonomous and [31] for nonautonomous systems. Persistence of homoclinic orbits under time discretization has been analyzed in [52, Theorem 4.3] and [23, Theorem 4.2].

Homoclinic orbits are of great dynamical relevance. For autonomous discrete time systems, it is well known that in the maximal invariant neighborhood of a homoclinic orbit, the dynamics are conjugate to a subshift on bi-infinite sequences. This symbolic dynamical system is a prototype for chaotic dynamics. We refer to the famous theorem of Smale [50] and Shilnikov [49] and to the articles [51] and [7] for recent discussions of the symbolic coding in infinite time. The latter reference also considers the finite time case, including numerical techniques

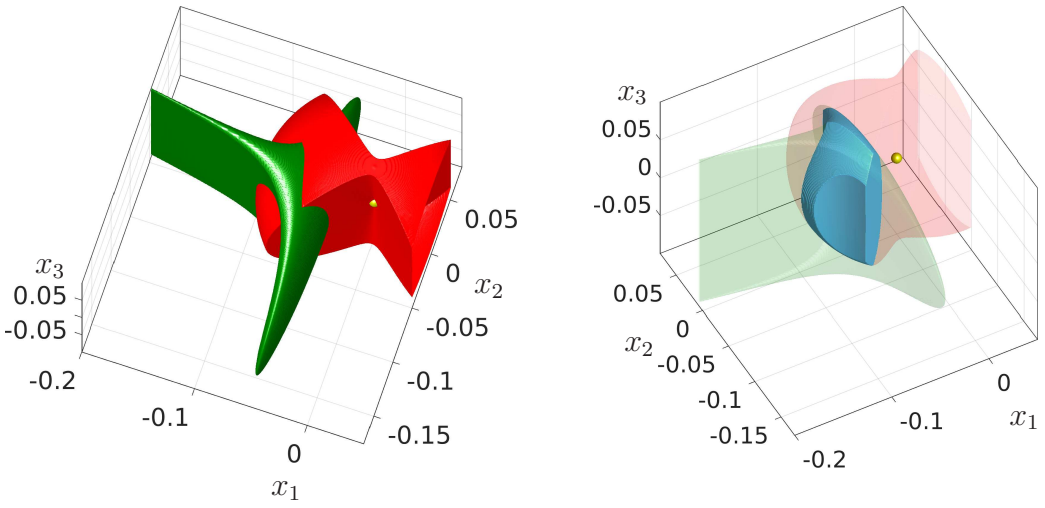

Figure 6: The left panel shows an approximation of $\mathcal{W}^s_\varepsilon(0,t)$ (green) and of $\mathcal{W}^u_\varepsilon(0,t)$ (red) for (24) for $t = 2.5 - h$. The intersection of these sets (blue) is illustrated in the right panel.

that provide an approximation of the maximal invariant set.

Let $\tilde{\mathbb{T}}$ be a bounded time interval in discrete or continuous time. An orbit $\bar{x}_{\tilde{\mathbb{T}}}$ of the finite time dynamical system $(\mathbb{R}^d, \tilde{\mathbb{T}}, \Psi)$ is homoclinic w.r.t. the reference trajectory $\xi_{\tilde{\mathbb{T}}}$ if

$$\bar{x}(t) \in \mathcal{W}^s_\varepsilon(\xi_{\tilde{\mathbb{T}}}, t) \cap \mathcal{W}^u_\varepsilon(\xi_{\tilde{\mathbb{T}}}, t) \quad \text{for all } t \in (t_-, t_+)_{\tilde{\mathbb{T}}}.$$

Homoclinic orbits of infinite time dynamical systems result in finite time homoclinic orbits for a finite time restriction of the system, under two additional assumptions. First, the homoclinic orbit must eventually converge monotonously towards the reference trajectory and secondly, these orbits must reach the ε-neighborhood within the finite time horizon.

Formally, we assume on the infinite time interval $\mathbb{T}$ without loss of generality that $\xi(t) = 0$ for all $t \in \mathbb{T}$, which can be achieved by a nonautonomous Lyapunov transformation. In an $\bar{\varepsilon}$-neighborhood of 0, points on the stable fiber bundle at time $t \in \mathbb{T}$ have the graph representation $x = x_s + h^s_t(x_s)$, where x_s lies in the stable subspace at time t of the exponential dichotomy and $h^s_t(0) = 0$, $Dh^s_t(0) = 0$, see [1, Theorem 4.1]. A corresponding graph representation also exists for points on the unstable fiber bundle: $x = x_u + h^u_t(x_u)$ for $t \in \mathbb{T}$.

We state the following assumptions on the infinite time dynamical systems (1) and (3).

(A1) The fixed point 0 is M-hyperbolic in the sense of Definition 1.

(A2) $\bar{x}_{\mathbb{T}}$ is a homoclinic orbit w.r.t. the fixed point 0 of Ψ.

(A3) There exists a $C > 0$ such that $\Psi(t, s; x) = \Phi(t, s)x + g(t, s, x)$, where $\|g(t, s, x)\| \leq C\|x\|^2$ for all $x \in \mathcal{B}_{\bar{\varepsilon}}(0)$ and all $s, t \in \mathbb{T}$ such that $|t - s| \leq 1$.

(A4) $\|\Phi(t,s)\| \le C$ for all $s,t \in \mathbb{T}$ such that $|t-s| \le 1$.

(A5) $\|h_t^{s,u}(x)\| \le C\|x\|^2$ for all $t \in \mathbb{T}$ and $x \in \mathcal{B}_{\bar\varepsilon}(0)$.

(A6) The (possibly nonautonomous) norm satisfies $\|x_{s,u}(t)\| \le \|x(t)\|$ for all $x(t) = x_s(t) + x_u(t) \in \mathcal{B}_{\bar\varepsilon}(0)$, where $x_{s,u}(t)$ lies in the stable respectively unstable subspace of the exponential dichotomy at time $t \in \mathbb{T}$.

Theorem 6 *Let the assumptions (A1)-(A6) be satisfied. Then there exists an $\tilde\varepsilon > 0$ such that for any $0 < \varepsilon < \tilde\varepsilon$, there is an $\bar N$ such that for all $N \ge \bar N$, $\mathbb{T}_N := [-N,N]_{\mathbb{T}}$ it follows that $\bar x_{\mathbb{T}_N}$ is a finite time homoclinic orbit of the system $(\mathbb{R}^d, \mathbb{T}_N, \Psi)$ w.r.t. the fixed point 0.*

Proof: First, we verify monotonicity of the homoclinic orbit $\bar x_{\mathbb{T}}$ in a sufficiently small neighborhood of 0. With $\bar\varepsilon$ from (A3), one finds an $\bar s \in \mathbb{T}$ such that $\bar x(t) \in \mathcal{B}_{\bar\varepsilon}(0)$ for all $t \in \mathbb{T}$, $t \ge \bar s$. We conclude for all $t,s \in \mathbb{T}$, $t = s+1 > s > \bar s$ that

$$\begin{aligned}
\|\Psi(t,s;\bar x(s))\| &\le \|\Phi(t,s)\bar x(s)\| + \|g(t,s,\bar x(s))\| \\
&\le \|\Phi(t,s)\bar x_s(s)\| + \|\Phi(t,s)h_s^s(\bar x_s(s))\| + \|g(t,s,\bar x(s))\| \\
&\le \mathrm{e}^{-\alpha_s(t-s)}\|\bar x_s(s)\| + C\|\bar x_s(s)\|^2 + C\|\bar x(s)\|^2 \\
&\le \left(\mathrm{e}^{-\alpha_s} + 2C\|\bar x(s)\|\right)\|\bar x(s)\| \\
&< \|\bar x(s)\|
\end{aligned}$$

for $0 < \tilde\varepsilon \le \bar\varepsilon$ sufficiently small and $\bar x(s) \in \mathcal{B}_{\tilde\varepsilon}(0)$. A similar computation proves monotone convergence for $t \to -\infty$, provided $\tilde\varepsilon$ is decreased even further.

Thus, we find for each $0 < \varepsilon < \tilde\varepsilon$ an $\bar N$ such that the endpoints of the homoclinic orbit $\bar x_{\mathbb{T}_N}$ lie in $\mathcal{B}_\varepsilon(0)$ for all $N \ge \bar N$. As a consequence, $\bar x_{\mathbb{T}_N}$ lies in the intersection of finite time areas of attraction and repulsion of the fixed point 0. ■

Homoclinic points of (24) at time $t = 2.5 - h$ are located in the blue area, shown in Figure 6. The assumptions of Theorem 6 are satisfied for this example. However, the variational equation (4) along this homoclinic orbit does not possess an exponential dichotomy in the sense of Definition 1. A dichotomy estimate of the form (5) only holds, if a reasonably small constant $K > 1$ is accepted on the right hand side of (5).

In finite time models, homoclinic orbits are not isolated. It follows from [7, Theorem 8] that the distance between two homoclinic orbits shrinks exponentially fast towards the midpoint of the finite time interval. The homoclinic areas that are shown in Figure 5 clearly illustrate this characteristic.

Finally, we note that the occurrence of homoclinic chaos in nonautonomous discrete time systems – on infinite time intervals – depends on the way in which stable and unstable sets intersect each other, cf. [39]. The main reason for non-chaotic dynamics near homoclinic orbits constitutes the observation that stable and unstable fibers may intersect only once in an isolated point, see [23] for more details. We introduce a finite time example of this type in the next section.

4.2 A nonautonomous nonlinear model

We consider the following model for homoclinic dynamics from [23, Section 5.1]:

$$\begin{pmatrix} x_1 \\ x_2 \end{pmatrix}' = \begin{pmatrix} x_2 + x_1^2 + 6x_1 \mathrm{sech}^2(t) \\ x_1^2 + 4x_1 + x_2^2 - 12x_2 \mathrm{sech}^2(t)\tanh(t) \end{pmatrix}. \tag{25}$$

With respect to the finite time interval $\mathbb{T} = [-1.5, 1.5]$, we compute areas of attraction and repulsion of the hyperbolic fixed point 0 at $t = -1$ and $t = -0.5$. We choose $\varepsilon \in \{1.8, 2, 2.2\}$ rather large. This setting guarantees an intersection of stable and unstable sets on the short time interval $\mathbb{T}$. In Figure 7, these sets and their intersections are computed. We apply the classical Runge-Kutta scheme for discretizing the ODE (25) with step size $h = 0.01$.

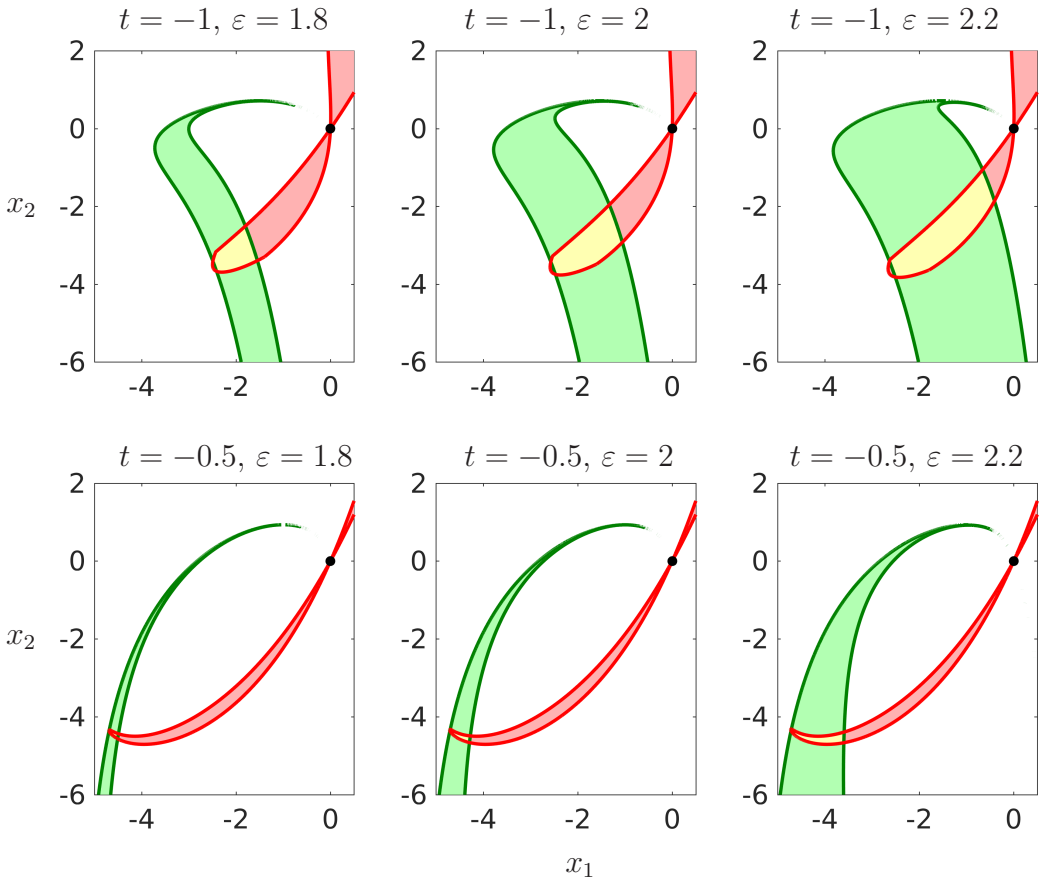

Figure 7: Approximation of $\mathcal{W}^s_\varepsilon(0,t)$ (green) and of $\mathcal{W}^u_\varepsilon(0,t)$ (red) for (25). Homoclinic points lie in the intersection of these sets (yellow).

During this computation, we have to verify monotonicity in the ε-neighborhood of 0 in each step. Unlike the autonomous case, it does not suffice to verify monotonicity in the last step only, since Lemma 5 does not apply to nonautonomous models.

The width of the green sets shrinks in a neighborhood of the fixed point and we cannot expect to detect these narrow areas by computing the zero contour of

$$\begin{aligned}\hat{G}^s_\varepsilon(z,t) \;:=\; &\min\{\varepsilon - \|\Psi(t_+ - h, t; z)\|,\\ &\|\Psi(s,t;z)\| - \|\Psi(s+h,t;z)\| : m^s(0,\varepsilon,z,t) \le s \le t_+ - h\},\end{aligned}$$

where m^s is defined in (7). For this task, points from the chosen 2000×2000 grid have to lie inside and outside of the contour, which is not satisfied in a neighborhood of 0. Alternatively, one may apply techniques for infinite time dynamical systems to compute this nearly one-dimensional part of the stable set. The contour-algorithm from [32, 33] provides an approximation of invariant fiber bundles for infinite time systems. We apply this algorithm for computing parts of Figure 5.

5 Conclusion

In finite time dynamical systems, the absence of an infinite limit process leads to several meaningful, but nonequivalent definitions of areas of attraction and repulsion. The definition proposed here is based on two characteristics: ε-closeness of the end points to the reference trajectory and eventual monotonicity. This ansatz allows numerical computations, since the boundaries of these areas are essentially the zero-set of specific operators. By evaluating these operators numerically and applying the MATLAB-routines `contour` and `isosurface` we obtain a graphical representation of areas of attraction and repulsion. These techniques apply to autonomous and nonautonomous dynamical systems. Calculations in the nonautonomous case are slightly more expensive, since the test for monotonicity is more involved. Intersections of areas of attraction and repulsion reveal homoclinic points that are of great dynamical relevance. For an illustration, we choose two- and three-dimensional models in discrete and continuous time. We note that our techniques also apply to higher dimensional models and enable the computation of two- and three-dimensional projections, see [34, Section 3.6] for corresponding calculations in infinite time dynamical systems.

References

[1] B. Aulbach. The fundamental existence theorem on invariant fiber bundles. *J. Differ. Equations Appl.*, 3(5-6):501–537, 1998.

[2] B. Aulbach and J. Kalkbrenner. Exponential forward splitting for noninvertible difference equations. *Comput. Math. Appl.*, 42(3-5):743–754, 2001. Advances in difference equations, III.

[3] L. Barreira and Y. B. Pesin. *Lyapunov exponents and smooth ergodic theory*, volume 23 of *University Lecture Series*. American Mathematical Society, Providence, RI, 2002.

[4] A. Berger, T. Doan, and S. Siegmund. A remark on finite-time hyperbolicity. *PAMM*, 8(1):10917–10918, 2008.

[5] A. Berger, T. S. Doan, and S. Siegmund. A definition of spectrum for differential equations on finite time. *J. Differential Equations*, 246(3):1098–1118, 2009.

[6] A. Berger, D. T. Son, and S. Siegmund. Nonautonomous finite-time dynamics. *Discrete Contin. Dyn. Syst. Ser. B*, 9(3-4):463–492, 2008.

[7] W.-J. Beyn, T. Hüls, and A. Schenke. Symbolic coding for noninvertible systems: Uniform approximation and numerical computation. *Nonlinearity*, 29:3346–3384, 2016.

[8] W.-J. Beyn and W. Kleß. Numerical Taylor expansions of invariant manifolds in large dynamical systems. *Numer. Math.*, 80(1):1–38, 1998.

[9] M. Branicki and S. Wiggins. Finite-time lagrangian transport analysis: stable and unstable manifolds of hyperbolic trajectories and finite-time lyapunov exponents. *Nonlinear Processes in Geophysics*, 17(1):1–36, 2010.

[10] X. Cabré, E. Fontich, and R. de la Llave. The parameterization method for invariant manifolds. III. Overview and applications. *J. Differential Equations*, 218(2):444–515, 2005.

[11] F. Colonius and W. Kliemann. *The dynamics of control*. Systems & Control: Foundations & Applications. Birkhäuser Boston, Inc., Boston, MA, 2000.

[12] W. A. Coppel. *Dichotomies in Stability Theory*. Springer-Verlag, Berlin, 1978. Lecture Notes in Mathematics, Vol. 629.

[13] J. L. Daleckiĭ and M. G. Kreĭn. *Stability of Solutions of Differential Equations in Banach Space*. American Mathematical Society, Providence, R.I., 1974.

[14] M. Dellnitz and A. Hohmann. A subdivision algorithm for the computation of unstable manifolds and global attractors. *Numer. Math.*, 75(3):293–317, 1997.

[15] T. S. Doan, D. Karrasch, T. Y. Nguyen, and S. Siegmund. A unified approach to finite-time hyperbolicity which extends finite-time Lyapunov exponents. *J. Differential Equations*, 252(10):5535–5554, 2012.

[16] T. S. Doan, K. Palmer, and S. Siegmund. Transient spectral theory, stable and unstable cones and Gershgorin's theorem for finite-time differential equations. *J. Differential Equations*, 250(11):4177–4199, 2011.

[17] E. J. Doedel, B. Krauskopf, and H. M. Osinga. Global organization of phase space in the transition to chaos in the Lorenz system. *Nonlinearity*, 28(11):R113–R139, 2015.

[18] L. H. Duc and S. Siegmund. Hyperbolicity and invariant manifolds for planar nonautonomous systems on finite time intervals. *Internat. J. Bifur. Chaos Appl. Sci. Engrg.*, 18(3):641–674, 2008.

[19] T. Eirola and J. von Pfaler. Numerical Taylor expansions for invariant manifolds. *Numer. Math.*, 99(1):25–46, 2004.

[20] S. Elaydi. *An introduction to difference equations*. Undergraduate Texts in Mathematics. Springer, New York, third edition, 2005.

[21] J. P. England, B. Krauskopf, and H. M. Osinga. Computing one-dimensional stable manifolds and stable sets of planar maps without the inverse. *SIAM J. Appl. Dyn. Syst.*, 3(2):161–190 (electronic), 2004.

[22] P. Giesl and M. Rasmussen. Areas of attraction for nonautonomous differential equations on finite time intervals. *J. Math. Anal. Appl.*, 390(1):27–46, 2012.

[23] A. Girod and T. Hüls. Nonautonomous systems with transversal homoclinic structures under discretization. *BIT*, 56(2):605–631, 2016.

[24] G. Haller. Finding finite-time invariant manifolds in two-dimensional velocity fields. *Chaos*, 10(1):99–108, 2000.

[25] G. Haller. Lagrangian structures and the rate of strain in a partition of two-dimensional turbulence. *Phys. Fluids*, 13(11):3365–3385, 2001.

[26] G. Haller and T. Sapsis. Lagrangian coherent structures and the smallest finite-time Lyapunov exponent. *Chaos*, 21(2):023115, 7, 2011.

[27] À. Haro, M. Canadell, J.-L. Figueras, A. Luque, and J.-M. Mondelo. *The parameterization method for invariant manifolds – From rigorous results to effective computations*, volume 195 of *Applied Mathematical Sciences*. Springer, 2016.

[28] D. Henry. *Geometric Theory of Semilinear Parabolic Equations*. Springer-Verlag, Berlin, 1981.

[29] T. Hüls. Numerical computation of dichotomy rates and projectors in discrete time. *Discrete Contin. Dyn. Syst. Ser. B*, 12(1):109–131, 2009.

[30] T. Hüls. Computing Sacker-Sell spectra in discrete time dynamical systems. *SIAM J. Numer. Anal.*, 48(6):2043–2064, 2010.

[31] T. Hüls. Homoclinic trajectories of non-autonomous maps. *J. Difference Equ. Appl.*, 17(1):9–31, 2011.

[32] T. Hüls. A contour algorithm for computing stable fiber bundles of nonautonomous, noninvertible maps. *SIAM J. Appl. Dyn. Syst.*, 15(2):923–951, 2016.

[33] T. Hüls. On the Approximation of Stable and Unstable Fiber Bundles of (Non)Autonomous ODEs — A Contour Algorithm. *Internat. J. Bifur. Chaos Appl. Sci. Engrg.*, 26(7):1650118, 10, 2016.

[34] T. Hüls. Computing stable hierarchies of fiber bundles. *Discrete Contin. Dyn. Syst. Ser. B*, 2017. DOI: 10.3934/dcdsb.2017140.

[35] J. Kalkbrenner. *Exponentielle Dichotomie und chaotische Dynamik nichtinvertierbarer Differenzengleichungen*, volume 1 of *Augsburger Mathematisch-Naturwissenschaftliche Schriften*. Dr. Bernd Wißner, Augsburg, 1994.

[36] D. Karrasch. Linearization of hyperbolic finite-time processes. *J. Differential Equations*, 254(1):256–282, 2013.

[37] P. E. Kloeden and M. Rasmussen. *Nonautonomous dynamical systems*, volume 176 of *Mathematical Surveys and Monographs*. American Mathematical Society, Providence, RI, 2011.

[38] B. Krauskopf, H. M. Osinga, E. J. Doedel, M. E. Henderson, J. Guckenheimer, A. Vladimirsky, M. Dellnitz, and O. Junge. A survey of methods for computing (un)stable manifolds of vector fields. *Internat. J. Bifur. Chaos Appl. Sci. Engrg.*, 15(3):763–791, 2005.

[39] L. M. Lerman and L. P. Shil′nikov. Homoclinical structures in nonautonomous systems: nonautonomous chaos. *Chaos*, 2(3):447–454, 1992.

[40] C. Lopesino, F. Balibrea, S. Wiggins, and A. M. Mancho. Lagrangian descriptors for two dimensional, area preserving, autonomous and nonautonomous maps. *Commun. Nonlinear Sci. Numer. Simul.*, 27(1-3):40–51, 2015.

[41] A. M. Mancho, D. Small, S. Wiggins, and K. Ide. Computation of stable and unstable manifolds of hyperbolic trajectories in two-dimensional, aperiodically time-dependent vector fields. *Phys. D*, 182(3-4):188–222, 2003.

[42] K. J. Palmer. Exponential dichotomies, the shadowing lemma and transversal homoclinic points. In *Dynamics reported, Vol. 1*, pages 265–306. Teubner, Stuttgart, 1988.

[43] O. Perron. Die Stabilitätsfrage bei Differentialgleichungen. *Math. Z.*, 32(1):703–728, 1930.

[44] C. Pötzsche. *Geometric theory of discrete nonautonomous dynamical systems*, volume 2002 of *Lecture Notes in Mathematics*. Springer-Verlag, Berlin, 2010.

[45] C. Pötzsche and M. Rasmussen. Taylor approximation of invariant fiber bundles for nonautonomous difference equations. *Nonlinear Anal.*, 60(7):1303–1330, 2005.

[46] C. Pötzsche and M. Rasmussen. Computation of nonautonomous invariant and inertial manifolds. *Numer. Math.*, 112(3):449–483, 2009.

[47] S. C. Shadden, F. Lekien, and J. E. Marsden. Definition and properties of Lagrangian coherent structures from finite-time Lyapunov exponents in two-dimensional aperiodic flows. *Phys. D*, 212(3-4):271–304, 2005.

[48] M. Shub. *Global stability of dynamical systems*. Springer-Verlag, New York, 1987.

[49] L. P. Šil′nikov. On a problem of Poincaré-Birkhoff. *Mat. Sb. (N.S.)*, 74 (116):378–397, 1967.

[50] S. Smale. Differentiable dynamical systems. *Bull. Amer. Math. Soc.*, 73:747–817, 1967.

[51] H. Steinlein and H.-O. Walther. Hyperbolic sets, transversal homoclinic trajectories, and symbolic dynamics for C^1-maps in Banach spaces. *J. Dynam. Differential Equations*, 2(3):325–365, 1990.

[52] Y.-K. Zou and W.-J. Beyn. On manifolds of connecting orbits in discretizations of dynamical systems. *Nonlinear Anal.*, 52(5):1499–1520, 2003.